

## A HIGH STELLAR VELOCITY DISPERSION AND $\sim 100$ GLOBULAR CLUSTERS FOR THE ULTRA DIFFUSE GALAXY DRAGONFLY 44

PIETER VAN DOKKUM<sup>1</sup>, ROBERTO ABRAHAM<sup>2</sup>, JEAN BRODIE<sup>3</sup>, CHARLIE CONROY<sup>4</sup>, SHANY DANIELI<sup>1</sup>, ALLISON MERRITT<sup>1</sup>, LAMIYA MOWLA<sup>1</sup>, AARON ROMANOWSKY<sup>3,5</sup>, JIELAI ZHANG<sup>2</sup>

*Accepted for publication in ApJ Letters*

### ABSTRACT

Recently a population of large, very low surface brightness, spheroidal galaxies was identified in the Coma cluster. The apparent survival of these Ultra Diffuse Galaxies (UDGs) in a rich cluster suggests that they have very high masses. Here we present the stellar kinematics of Dragonfly 44, one of the largest Coma UDGs, using a 33.5 hr integration with DEIMOS on the Keck II telescope. We find a velocity dispersion of  $\sigma = 47_{-6}^{+8}$  km s<sup>-1</sup>, which implies a dynamical mass of  $M_{\text{dyn}}(< r_{1/2}) = 0.7_{-0.2}^{+0.3} \times 10^{10} M_{\odot}$  within its deprojected half-light radius of  $r_{1/2} = 4.6 \pm 0.2$  kpc. The mass-to-light ratio is  $M/L_I(< r_{1/2}) = 48_{-14}^{+21} M_{\odot}/L_{\odot}$ , and the dark matter fraction is 98% within  $r_{1/2}$ . The high mass of Dragonfly 44 is accompanied by a large globular cluster population. From deep Gemini imaging taken in 0".4 seeing we infer that Dragonfly 44 has  $94_{-20}^{+25}$  globular clusters, similar to the counts for other galaxies in this mass range. Our results add to other recent evidence that many UDGs are “failed” galaxies, with the sizes, dark matter content, and globular cluster systems of much more luminous objects. We estimate the total dark halo mass of Dragonfly 44 by comparing the amount of dark matter within  $r = 4.6$  kpc to enclosed mass profiles of NFW halos. The enclosed mass suggests a total mass of  $\sim 10^{12} M_{\odot}$ , similar to the mass of the Milky Way. The existence of nearly-dark objects with this mass is unexpected, as galaxy formation is thought to be maximally-efficient in this regime.

*Keywords:* galaxies: clusters: individual (Coma) — galaxies: evolution — galaxies: structure

### 1. INTRODUCTION

Deep imaging of the Coma cluster with the Dragonfly Telescope Array (Abraham & van Dokkum 2014) uncovered a substantial population of intrinsically-large, very low surface brightness galaxies (van Dokkum et al. 2015a). These Ultra Diffuse Galaxies (UDGs) have central surface brightnesses  $\mu(g, 0) > 24$  mag arcsec<sup>-2</sup> and projected half-light radii  $R_e > 1.5$  kpc. UDGs are fairly red, relatively round, and featureless; visually, and in their central surface brightness, they resemble dwarf spheroidal galaxies such as Sculptor and Draco, except that their half-light radii are more than an order of magnitude larger. Individual examples of such galaxies had been known for many years (Impey, Bothun, & Malin 1988; Dalcanton et al. 1997), but their ubiquity, at least in dense environments (van Dokkum et al. 2015a; Koda et al. 2015; van der Burg, Muzzin, & Hoekstra 2016; Roman & Trujillo 2016), had not been recognized.

It is not clear how UDGs are related to other classes of galaxies. One possibility is that they are the result of processing by the cluster environment, and either started out as small, low mass galaxies or as very extended, low surface brightness disks (see, e.g., Moore et al. 1996; Hayashi et al. 2003; Gnedin 2003; Collins et al. 2013; Yozin & Bekki 2015). It has been suggested that tides were responsible for creating some of the largest and faintest galaxies in the Local Group

(Collins et al. 2013), and these processes are expected to be particularly effective in clusters (Moore et al. 1996; Yozin & Bekki 2015). Another idea is that UDGs represent the most rapidly-rotating tail of the distribution of dwarf galaxies, as the size and surface brightness of a galaxy are thought to be related to its spin (Amorisco & Loeb 2016). The axis ratio distribution of UDGs is inconsistent with disks under random viewing angles (van Dokkum et al. 2015a), but Amorisco & Loeb (2016) suggested that this could be the result of processing by the cluster environment (see also Gnedin 2003).

It may also be that UDGs, or a subset of them, are not closely related to other low luminosity galaxies but have more in common with galaxies that are typically much brighter. That is, it may be that UDGs are “failed” galaxies that were prevented from building a normal stellar population, because of extreme feedback from supernovae and young stars (Agertz & Kravtsov 2015; Calura et al. 2015), gas stripping (Fujita 2004; Yozin & Bekki 2015), AGN feedback (Reines et al. 2013), or other effects. Several recent studies have provided evidence for this interpretation, as UDGs appear to have globular cluster populations that are unusually rich for such faint galaxies (Beasley et al. 2016; Peng & Lim 2016; Beasley & Trujillo 2016). In particular, the galaxy Dragonfly 17 in the Coma cluster has  $\sim 30$  globular clusters despite its absolute magnitude of only  $M_V = -15.1$ , and could be interpreted as a “failed” LMC or M33 (Peng & Lim 2016; Beasley & Trujillo 2016). These extensive globular cluster populations suggest massive dark matter halos (Harris, Harris, & Alessi 2013; Beasley et al. 2016; Peng & Lim 2016), and are all the more remarkable when stripping by the cluster tidal field is taken into account (e.g., Smith et al. 2013).

Suggestive as the globular clusters are, it is difficult to interpret UDGs without measuring their masses. Reliable masses are needed to verify the assertion that the galaxies owe their

<sup>1</sup> Astronomy Department, Yale University, New Haven, CT 06511, USA

<sup>2</sup> Department of Astronomy & Astrophysics, University of Toronto, 50 St. George Street, Toronto, ON M5S 3H4, Canada

<sup>3</sup> University of California Observatories, 1156 High Street, Santa Cruz, CA 95064, USA

<sup>4</sup> Harvard-Smithsonian Center for Astrophysics, 60 Garden Street, Cambridge, MA, USA

<sup>5</sup> Department of Physics and Astronomy, San José State University, San Jose, CA 95192, USA

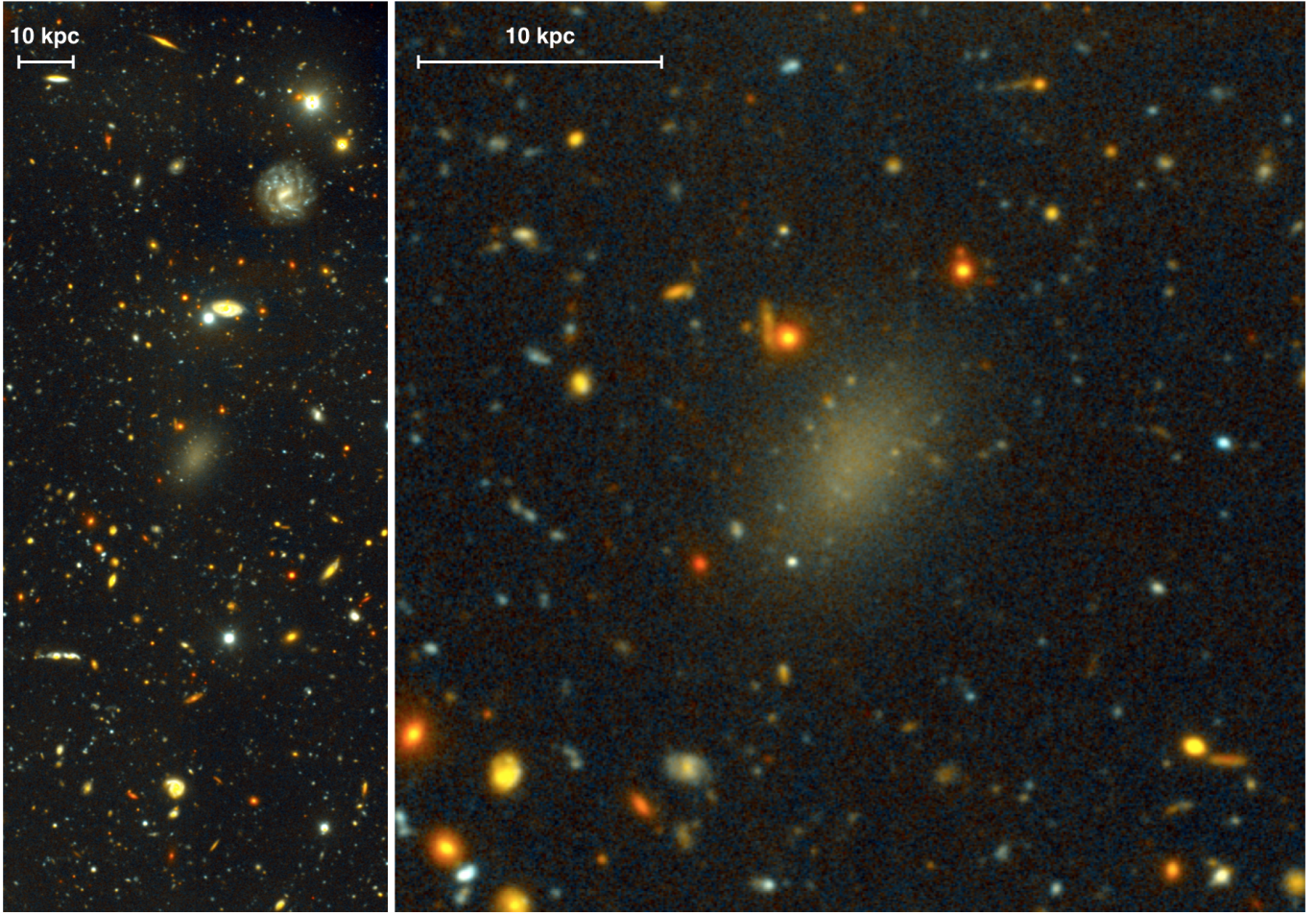


**Figure 1.** Deep Gemini  $g$  and  $i$  images were combined to create a color image of Dragonfly 44 and its immediate surroundings. The galaxy has a remarkable appearance: it is a low surface brightness, spheroidal object that is peppered with faint, compact sources.

structural stability to their high dark matter fractions (van Dokkum et al. 2015a), and can settle the question whether UDGs are truly distinct from other galaxies of the same luminosity. The first dynamical constraint on the mass of an UDG was obtained by Beasley et al. (2016), from the velocities of six globular clusters attributed to the faint ( $M_g = -13.3$ ) galaxy VCC 1287 in the Virgo cluster. The velocity dispersion of  $\sigma = 33^{+16}_{-10}$  km s $^{-1}$  suggests a halo mass of  $\sim 10^{11} M_\odot$ , although its large uncertainty leaves room for a range of interpretations (see Amorisco & Loeb 2016).

In this *Letter* we build on these previous studies with a measurement of the stellar dynamics of a UDG, based on extremely deep spectroscopy with the Deep Imaging Multi-Object Spectrograph (DEIMOS) on the Keck II telescope. We also provide a measurement of the globular cluster system of the galaxy, using ground-based imaging of exceptional quality obtained with the Gemini-North telescope. A distance of 101 Mpc is assumed.

## 2. STELLAR VELOCITY DISPERSION

### 2.1. Target Selection and Observations

Dragonfly 44 is the second-largest of the 47 UDGs that were found in our survey of the Coma cluster with the Dragonfly Telephoto Array. Morphologically it is similar to other UDGs. It is the only Coma UDG that has

been spectroscopically-confirmed as a cluster member (van Dokkum et al. 2015b), and one of only four UDGs that have a redshift from absorption lines.<sup>6</sup>

We obtained new imaging data for Dragonfly 44, using the Gemini-North telescope. The galaxy was observed on May 12, 2016 with the Gemini Multi-Object Spectrometer (GMOS) for a total of 3000 s in the  $g$ -band and 3000 s in the  $i$ -band. Conditions were excellent, and the delivered image quality is superb: the seeing is  $0.45''$  in  $g$  and  $0.40''$  in  $i$ . The data were reduced using standard techniques, making use of the tasks in the IRAF Gemini package. A color image of the galaxy and its immediate surroundings is shown in Fig. 1. There are no detected tidal features or other irregularities; previously reported variations in ellipticity (van Dokkum et al. 2015b) can be ascribed to compact sources (likely globular clusters, as discussed in Sect. 4) that were not recognized and masked in the earlier, relatively poor-seeing, data.

In order to measure the galaxy’s kinematics we observed it with the DEIMOS spectrograph on Keck II, using the 1200 lines mm $^{-1}$  grating. The slit width was  $1''0$  and the spectral resolution, as measured from sky emission lines, is  $\sigma_{\text{instr}} = 32$  km s $^{-1}$  near the redshifted H $\alpha$  line. The observations were carried out on January 15-16, March 11-12, and

<sup>6</sup> The others are two galaxies in Dalcanton et al. (1997) and the possible field UDG DGSAT1 (Martínez-Delgado et al. 2016).



April 9-10 2016, for a total integration time of 120,600 s (33.5 hrs). Conditions were excellent throughout. The central wavelength was  $\sim 6300 \text{ \AA}$ . Besides our main target three other UDGs fit in the multi-slit mask. One of these is the faint UDG Dragonfly 42; the other two were visually selected from archival CFHT imaging of the Coma cluster. Results for these three galaxies will be described elsewhere.

We developed a custom pipeline that is optimized for faint spatially-extended objects. Differences with the widely-used DEEP2 pipeline (Cooper et al. 2012) include a full modeling and subtraction of cross-talk; the use of sky lines rather than arc lines to create the distortion model; and a careful treatment of the background to avoid subtracting light from the large, diffuse targets during the reduction. The 2D spectrum and the collapsed 1D spectrum are shown in Fig. 2. The signal to noise ratio is 14 per  $0.32 \text{ \AA}$  pixel, corresponding to  $S/N = 21$  per resolution element. The dominant feature is the redshifted  $H\alpha$  absorption line.

## 2.2. Velocity Dispersion Measurement

The velocity dispersion was determined in the wavelength region  $6580 \text{ \AA} < \lambda < 6820 \text{ \AA}$ . The spectrum was fitted with high resolution stellar population synthesis models (Conroy, Gunn, & White 2009), using an implementation of the `emcee` Markov chain Monte Carlo sampler (Foreman-Mackey et al. 2013) to provide reliable errors that take parameter correlations into account. The fit finds the best linear combination of three templates, explicitly marginalizing over age and metallicity, and uses both multiplicative and additive polynomials to filter the continuum. After dividing them by the formal errors the residuals from the best fit have an rms scatter of  $\approx 1.0$ , which shows that the formal uncertainties correctly describe the true errors in the data.

We find a stellar line-of-sight velocity dispersion of  $\sigma = 47^{+8}_{-6} \text{ km s}^{-1}$ . The uncertainty in  $\sigma^2$ , which enters the dynamical mass, is 0.13 dex, considerably smaller than the uncertainty of 0.30 dex achieved for VCC 1287 by Beasley et al. (2016). There is no evidence for rotation; any systematic trend over  $\pm 5''$  is  $\Delta v < 10 \text{ km s}^{-1}$ , which implies that Dragonfly 44 is dispersion-dominated with  $v/\sigma \lesssim 0.2$ . There is also no evidence for radial variation in the velocity dispersion. To test the robustness of the best-fit dispersion we varied the templates and continuum filtering; masked the  $H\alpha$  line in the fit; split the data in four independent sets (the January run, the March run, and the two nights of the April run) and fitted those independently; and split the data in five spatial bins and fitted those independently. In all cases the best-fit dispersion (or the error-weighted combination of the independent fits) is well within  $1\sigma$  of our default value of  $47^{+8}_{-6} \text{ km s}^{-1}$ .

## 3. MASS AND MASS-TO-LIGHT RATIO INSIDE $R_{1/2}$

We combine the velocity dispersion with the projected half-light radius  $R_e$  to determine the dynamical mass and mass-to-light ( $M/L$ ) ratio of Dragonfly 44. We re-measured the half-light radius of Dragonfly 44 using the co-added  $g+i$  Gemini image. A 2D Sersic fit (Peng et al. 2002) gives  $R_e = 8.7'' \pm 0.3''$  (4.3 kpc at the distance of the Coma cluster), a Sersic index  $n = 0.85$ , and an axis ratio  $b/a = 0.66$ . These results are fully consistent with previous measurements for this galaxy (van Dokkum et al. 2015a, 2015b). The circularized projected half-light radius  $R_{e,c} = R_e \times \sqrt{b/a} = 3.5 \text{ kpc}$ , and the deprojected 3D circularized half-light radius  $r_{1/2} \approx 4/3 R_{e,c} = 4.6 \pm 0.2 \text{ kpc}$  (Wolf et al. 2010).

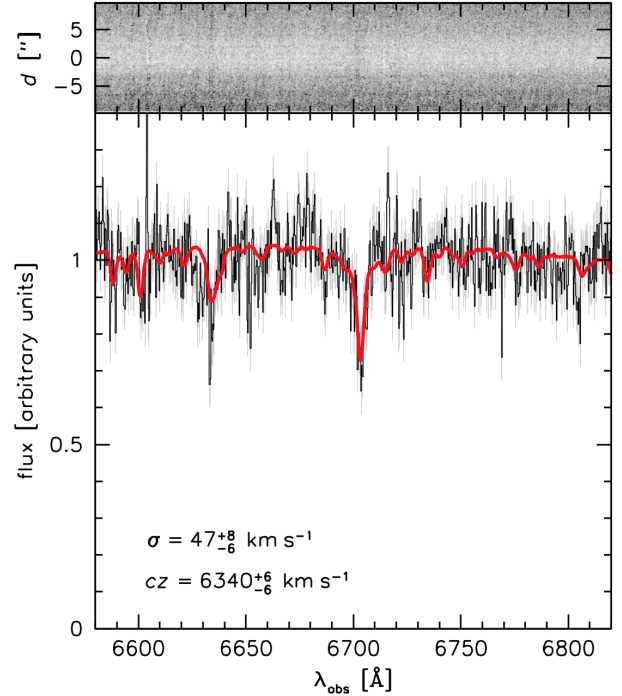


**Figure 2.** Deep (33.5 hr) spectrum of Dragonfly 44 obtained with DEIMOS on the Keck II telescope. The top panel shows the 2D spectrum. The main panel is the collapsed 1D spectrum, with the  $1\sigma$  uncertainties indicated in grey. A flexible model was fitted to the spectrum to determine the stellar velocity dispersion. The best-fitting model, with a dispersion  $\sigma = 47^{+8}_{-6} \text{ km s}^{-1}$ , is shown in red.

For dynamically-hot systems the luminosity-weighted stellar velocity dispersion, combined with the projected half-light radius  $R_e$ , strongly constrains the mass within the 3D half-light radius  $r_{1/2}$ :

$$M(r < r_{1/2}) \approx 9.3 \times 10^5 \sigma^2 R_e, \quad (1)$$

with  $M$  in  $M_\odot$ ,  $\sigma$  in  $\text{km s}^{-1}$  and  $R_e$  in kpc (Wolf et al. 2010). We find  $M(r < r_{1/2}) = 0.71^{+0.26}_{-0.17} \times 10^{10} M_\odot$ .

This mass is much higher than expected from the stellar population alone. Scaling the GALFIT model to the well-calibrated CFHT images of the galaxy (see van Dokkum et al. 2015a) and transforming from  $g$  and  $i$  to  $V$  and  $I$ , we find total magnitudes of  $M_V = -16.08$  and  $M_I = -17.11$  for Dragonfly 44. The mass-to-light ratio within  $r_{1/2}$  is  $M/L_I(r < r_{1/2}) = 48^{+21}_{-14} M_\odot/L_\odot$ . As shown in Fig. 3a, such high  $M/L$  ratios within the half-light radius are typical for very low mass dwarf galaxies and for galaxy clusters, but not for dispersion-dominated galaxies with the mass of Dragonfly 44.

We calculate the dark matter fraction inside  $r_{1/2}$  explicitly by assuming that the gas fraction is negligible. The stellar mass of Dragonfly 44, as determined from its  $i$ -band luminosity and  $g-i$  color (Taylor et al. 2011), is  $M_* \approx 3 \times 10^8 M_\odot$ . Therefore, the dark matter fraction inside  $r_{1/2}$  is  $f_{\text{dm}} = (M(r < r_{1/2}) - 0.5M_*)/M(r < r_{1/2}) \approx 98\%$ . This amount of dark matter is sufficient to prevent disruption of the galaxy by the Coma tidal field, at least at distances  $\gtrsim 100 \text{ kpc}$  from the center of the cluster (Gnedin 2003; van Dokkum et al. 2015a; van der Burg et al. 2016).

## 4. GLOBULAR CLUSTERS

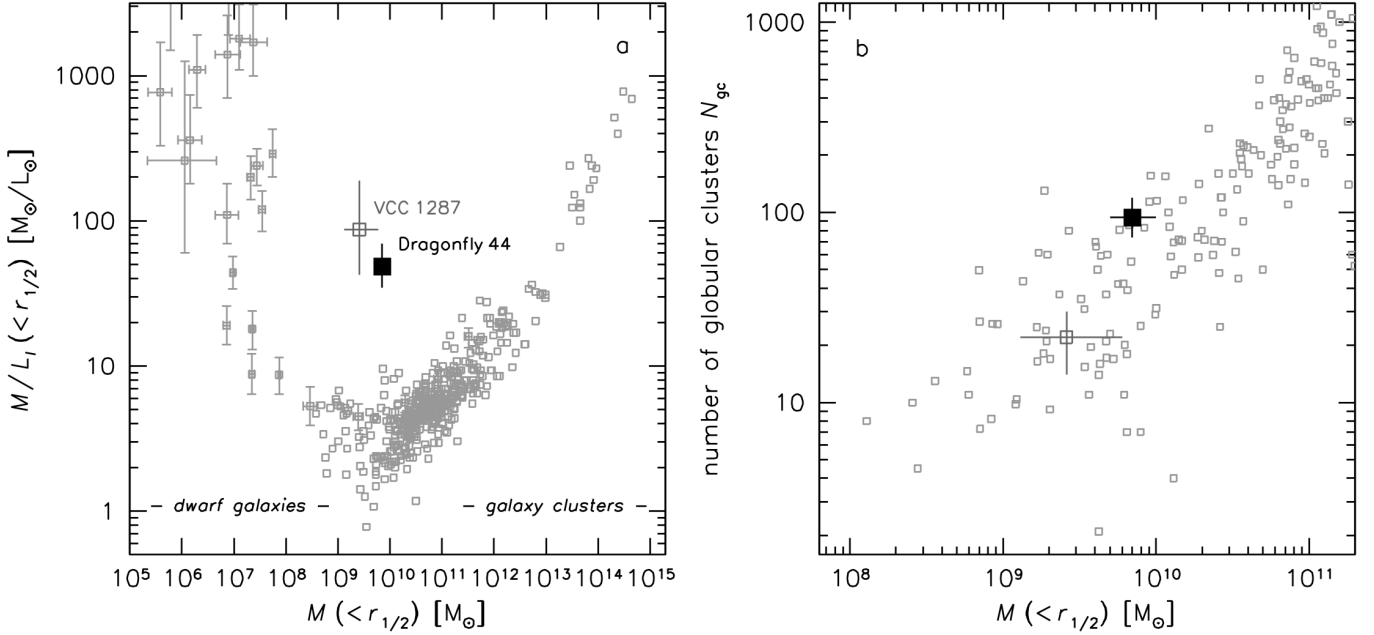


**Figure 3.** *a)* Relation between dynamical  $M/L_1$  ratio and dynamical mass. Open symbols are dispersion-dominated objects from Zaritsky, Gonzalez, & Zabludoff (2006) and Wolf et al. (2010). The UDGs VCC 1287 (Beasley et al. 2016) and Dragonfly 44 fall outside of the band defined by the other galaxies, having a very high  $M/L$  ratio for their mass. *b)* Relation between the number of globular clusters  $N_{gc}$  and dynamical mass. Open symbols are from the Harris et al. (2013) compilation. The UDGs are consistent with the relation defined by other galaxies in this luminosity-independent plane.

The high dynamical mass of Dragonfly 44 is accompanied by a remarkable population of compact sources, which we identify as globular clusters (see Fig. 1 and Fig. 4a). Figure 4b shows all compact objects with  $m_V \lesssim 28$  in the combined  $g+i$  image. They were identified with SExtractor (Bertin & Arnouts 1996) after subtracting a 2D ellipse fit to the galaxy. Large circles indicate objects brighter than the 80% completeness limit of  $m_V = 27.2$ .

The spatial distribution of the globular clusters is broadly similar to that of the galaxy light (see Fig. 4a), and we measure the number of compact objects within an ellipse that has the same orientation and axis ratio as the galaxy. It is well established that globular clusters have a more extended distribution than a galaxy’s stellar light (Kantha et al. 2014), and we assume that the half-“number” radius is  $R_{gc} = 1.5 \times R_e = 6.5$  kpc. This is a somewhat conservative estimate: well-studied luminous galaxies have  $R_{gc} \sim 1.8 \times R_e$  (Kantha et al. 2014), and Dragonfly 17 has  $R_{gc} \sim 1.7 \times R_e$  (Peng & Lim 2016). We find 35 compact objects within  $R_{gc}$ , 26 of which have  $m_V < 27.2$  (Fig. 4c). The red histogram in Fig. 4c is the expected magnitude distribution of unrelated compact objects, based on empty regions in the Gemini image. The background-corrected number of compact objects with  $R < R_{gc}$  and  $m_V < 27.2$  is 19.3, or 38.5 when including objects outside  $R = R_{gc}$ .

The luminosity function of globular clusters is well-approximated by a Gaussian (Harris et al. 2013), with a turnover magnitude of  $m_{V,cen} \approx 27.5$  at the distance of Coma (Miller & Lotz 2007; Lee & Jang 2016; Peng & Lim 2016). With 38.5 globular clusters having  $m_V < 27.2$ , we derive a total population of  $N_{gc} = 94^{+25}_{-20}$  (solid blue curve in Fig. 4d). The errors do not include systematic uncertainties. The Gemini images are sufficiently deep to provide a lower limit of  $m_{cen} \approx 27.2$ , and for this turnover magnitude we derive a total population of  $N_{gc} \approx 75$  (dashed blue curve in Fig. 4d). This

number is reduced further to  $N_{gc} \approx 63$  if we also assume that  $R_{gc} = R_e$  rather than  $1.5 \times R_e$ .

The preferred value of  $N_{gc} = 94$  is an order of magnitude larger than expected for galaxies with the luminosity of Dragonfly 44: the expected number of globular clusters for a galaxy with  $M_V = -16.1$  is  $N_{gc} = 8^{+14}_{-5}$ , where the error bars indicate 68% of the distribution in the Harris et al. (2013) compilation. The specific frequency is  $S_N = N_{gc} 10^{0.4(M_V+15)} = 35^{+9}_{-7}$ , similar to that of VCC 1287 and Dragonfly 17 (Beasley et al. 2016; Peng & Lim 2016; Beasley & Trujillo 2016). However, as shown in Fig. 3b, the number of globular clusters is similar to that of other galaxies with the same mass. The expected number of clusters for a galaxy with  $M_{dyn}(< r_{1/2}) = 0.7 \times 10^{10} M_\odot$  is  $36^{+60}_{-23}$ , which is not significantly different from the observed number. The difference would be even smaller if we had corrected the Harris et al. (2013) data points for the (large) contribution of baryons to the mass within  $r_{1/2}$ .

## 5. DISCUSSION

We have shown that the UDG Dragonfly 44 not only has a large size for its luminosity, it also has an anomalously large dynamical mass and globular cluster population. These results effectively rule out the hypothesis that all UDGs are rapidly-rotating or puffed-up versions of other low luminosity galaxies (e.g., Amorisco & Loeb 2016). Instead, the few UDGs that have been studied in detail (Beasley et al. 2016; Peng & Lim 2016, and this study) appear to be “failed” equivalents of more massive galaxies: it is their low luminosity, and the lack of a classical disk and bulge, that is anomalous.

As noted in § 1 it is not yet understood what physical processes are responsible for halting or preventing star formation in UDGs. As these processes, and galaxy formation in general, are thought to be a strong function of halo mass (e.g., Croton et al. 2006; Dekel et al. 2009; Behroozi, Wechsler, & Conroy 2013; Moster, Naab, & White 2013), it is important

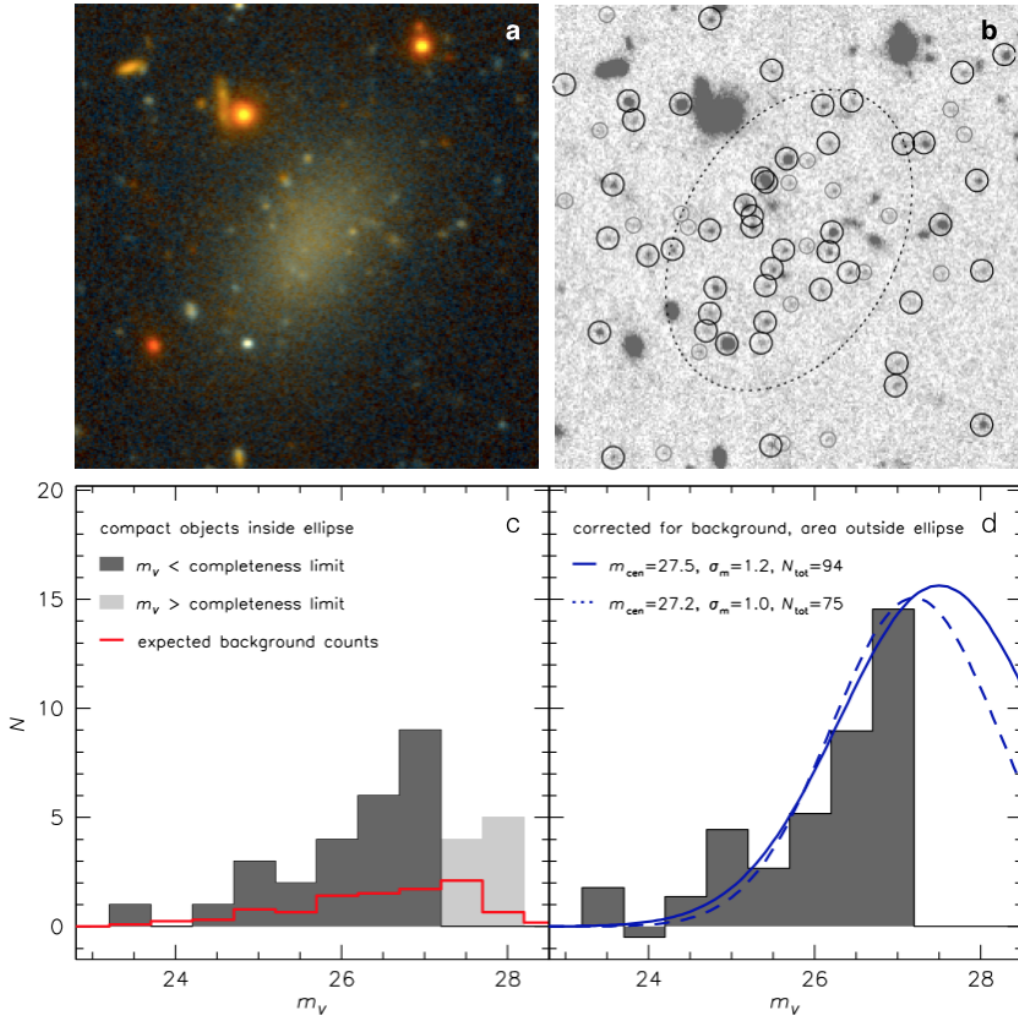


**Figure 4.** *a)* Enlargement of the color image shown in Fig. 1. *b)* Summed  $g$  and  $i$  image, after subtracting a 2D model for the galaxy. Black, large circles indicate compact objects brighter than the completeness limit. Grey circles are fainter objects. The broken ellipse indicates the assumed half-number semi-major axis of the globular clusters:  $R_{\text{gc}} = 1.5R_e = 6.5$  kpc. *c)* magnitude distribution of compact sources with  $R < R_{\text{gc}}$ . The red curve indicates the expected contribution from background objects. *d)* magnitude distribution brighter than the completeness limit, after subtracting the expected background and multiplying by two to include objects with  $R > R_{\text{gc}}$ . The blue curves are fits to the distribution for different assumptions for the turnover magnitude. For the expected turnover  $m_{\text{cen}} = 27.5$ , the total number of globular clusters is  $N_{\text{gc}} = 94_{-20}^{+25}$ .

to constrain the total amount of dark matter of Dragonfly 44. Following Beasley et al. (2016), we estimate the halo mass by comparing the enclosed mass within  $r_{1/2}$  to cumulative mass profiles of theoretical models. Beasley et al. (2016) assumed profiles from the EAGLE simulation (Crain et al. 2015), which include baryons. As UDGs are completely dominated by dark matter we use Navarro, Frenk, & White (1997) profiles instead, with a mass-dependent concentration  $c$  as parameterized by Macciò, Dutton, & van den Bosch (2008).

The results are shown in Fig. 5, for halos with  $M_{\text{halo}}(< r_{200}) = 10^{10} - 10^{13} M_{\odot}$ . The grey bands indicate the variation in the enclosed mass profiles for a halo-to-halo scatter in concentration of  $\Delta(\log c) = 0.14$ , and illustrate the degeneracy between concentration and derived halo mass (see, e.g., Taylor et al. 2015). The observed enclosed mass of Dragonfly 44 suggests a halo mass of  $M_{\text{halo}}(< r_{200}) \approx 8 \times 10^{11} M_{\odot}$ , if the halo has an average concentration and no truncation (see, e.g., Gnedin 2003, for a discussion of these assumptions).

Therefore, whereas VCC 1287 (and also Dragonfly 17) can

be considered “failed” LMCs or M33s, the more massive Dragonfly 44 can be viewed as a failed Milky Way. This distinction is potentially important: it is the accepted view that the ratio of stellar mass to halo mass reaches a peak of  $\sim 0.03$  for  $M_{\text{halo}} \sim 10^{12} M_{\odot}$ , which suggests that galaxy formation is maximally efficient in halos of this mass (Behroozi et al. 2013; Moster et al. 2013). Dragonfly 44 has a stellar mass that is a factor of  $\sim 100$  lower than expected in this framework, and in a standard halo abundance matching exercise it would be assigned the wrong halo mass.<sup>7</sup> More importantly, whatever physical processes are responsible for forming galaxies such as Dragonfly 44, they can apparently operate in a regime where galaxy formation was thought to be both maximally-efficient and relatively well understood.

We emphasize, however, that the halo abundance matching technique relies on total halo masses, and in our study the

<sup>7</sup> We note that this is based on the stellar mass – halo mass relation for field galaxies at  $z = 0$ ; as discussed in, e.g., Grossauer et al. (2015), the discrepancy may be smaller for cluster galaxies and if the galaxies formed at high redshift.

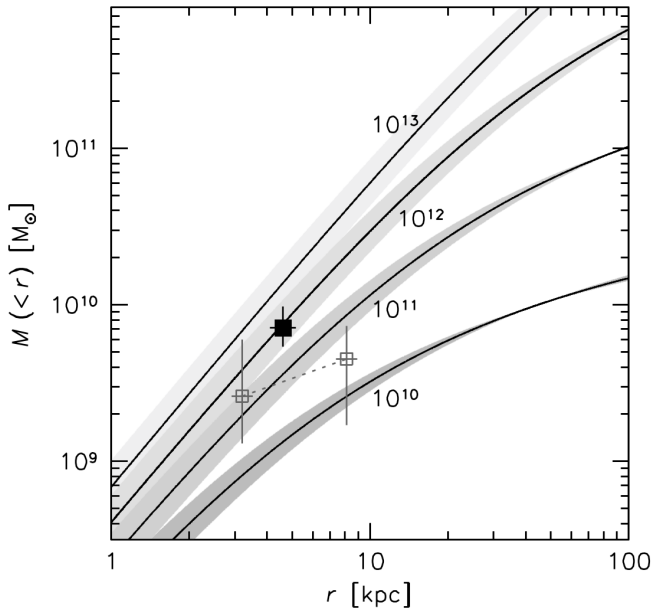


**Figure 5.** NFW halos (Navarro et al. 1997) with different masses within  $r_{200}$ . The black filled square is the enclosed mass of Dragonfly 44 within its deprojected half-light radius  $r_{1/2}$ . The light open squares are for VCC 1287; the two points are for  $r_{1/2}$  and for the radius that includes all six globular clusters with measured velocities (see Beasley et al. 2016).

total halo mass is an extrapolation of the measured mass by a factor of  $\sim 100$ . A more robust and less model-dependent conclusion is that the dark matter mass within  $r = 4.6$  kpc is similar to the dark matter mass of the Milky Way within the same radius (Xue et al. 2008). Better constraints on the halo masses of UDGs may come from lensing studies of large samples. Intriguingly, a weak lensing map of the Coma cluster by Okabe et al. (2014) shows a  $2\sigma$  peak at the location of Dragonfly 44. Peaks of similar significance have inferred masses of a few  $\times 10^{12} M_{\odot}$ , and unlike most other features in the map it is not associated with known bright galaxies or background structures.

Our study demonstrates that it is possible to measure the stellar kinematics of UDGs using existing instrumentation on large telescopes. With sufficiently large samples it will be possible to determine what fraction of UDGs are “failed” galaxies (as opposed to, say, tidally-stretched low mass galaxies), and what the variation is in their masses and  $M/L$  ratios. A preliminary analysis of the other, smaller, UDGs in our DEIMOS mask suggests that they have lower velocity dispersions than Dragonfly 44; a study of the ensemble of UDGs is in preparation.

We thank the anonymous referee for insightful comments which improved the manuscript.

## REFERENCES

- Abraham, R. G. & van Dokkum, P. G. 2014, *PASP*, 126, 55  
Agertz, O. & Kravtsov, A. V. 2015, arXiv:1509.00853  
Amorisco, N. C. & Loeb, A. 2016, *MNRAS*, 459, L51  
Beasley, M. A., Romanowsky, A. J., Pota, V., Navarro, I. M., Martínez-Delgado, D., Neyer, F., & Deich, A. L. 2016, *ApJ*, 819, L20  
Beasley, M. A. & Trujillo, I. 2016, arXiv:1604.08024  
Behroozi, P. S., Wechsler, R. H., & Conroy, C. 2013, *ApJ*, 770, 57  
Bertin, E. & Arnouts, S. 1996, *A&AS*, 117, 393  
Calura, F., Few, C. G., Romano, D., & D’Ercole, A. 2015, *ApJ*, 814, L14  
Collins, M. L. M., Chapman, S. C., Rich, R. M., Ibata, R. A., Martin, N. F., Irwin, M. J., Bate, N. F., Lewis, G. F., et al. 2013, *ApJ*, 768, 172  
Conroy, C., Gunn, J. E., & White, M. 2009, *ApJ*, 699, 486  
Cooper, M. C., Newman, J. A., Davis, M., Finkbeiner, D. P., & Gerke, B. F. 2012, spec2d: DEEP2 DEIMOS Spectral Pipeline, Astrophysics Source Code Library  
Crain, R. A., Schaye, J., Bower, R. G., Furlong, M., Schaller, M., Theuns, T., Dalla Vecchia, C., Frenk, C. S., et al. 2015, *MNRAS*, 450, 1937  
Croton, D. J., Springel, V., White, S. D. M., De Lucia, G., Frenk, C. S., Gao, L., Jenkins, A., Kauffmann, G., et al. 2006, *MNRAS*, 365, 11  
Dalcanton, J. J., Spergel, D. N., Gunn, J. E., Schmidt, M., & Schneider, D. P. 1997, *AJ*, 114, 635  
Dekel, A., Birnboim, Y., Engel, G., Freundlich, J., Goerdt, T., Mumcuoglu, M., Neistein, E., Pichon, C., et al. 2009, *Nature*, 457, 451  
Foreman-Mackey, D., Hogg, D. W., Lang, D., & Goodman, J. 2013, *PASP*, 125, 306  
Fujita, Y. 2004, *PASJ*, 56, 29  
Gnedin, O. Y. 2003, *ApJ*, 589, 752  
Grossauer, J., Taylor, J. E., Ferrarese, L., MacArthur, L. A., Côté, P., Roediger, J., Courteau, S., Cuillandre, J.-C., et al. 2015, *ApJ*, 807, 88  
Harris, W. E., Harris, G. L. H., & Alessi, M. 2013, *ApJ*, 772, 82  
Hayashi, E., Navarro, J. F., Taylor, J. E., Stadel, J., & Quinn, T. 2003, *ApJ*, 584, 541  
Impey, C., Bothun, G., & Malin, D. 1988, *ApJ*, 330, 634  
Kartha, S. S., Forbes, D. A., Spitler, L. R., Romanowsky, A. J., Arnold, J. A., & Brodie, J. P. 2014, *MNRAS*, 437, 273  
Koda, J., Yagi, M., Yamanoi, H., & Komiyama, Y. 2015, *ApJ*, 807, L2  
Lee, M. G. & Jang, I. S. 2016, *ApJ*, 819, 77  
Macciò, A. V., Dutton, A. A., & van den Bosch, F. C. 2008, *MNRAS*, 391, 1940  
Martínez-Delgado, D., Läsker, R., Sharina, M., Toloba, E., Fliri, J., Beaton, R., Valls-Gabaud, D., Karachentsev, I. D., et al. 2016, *AJ*, 151, 96  
Miller, B. W. & Lotz, J. M. 2007, *ApJ*, 670, 1074  
Moore, B., Katz, N., Lake, G., Dressler, A., & Oemler, A. 1996, *Nature*, 379, 613  
Moster, B. P., Naab, T., & White, S. D. M. 2013, *MNRAS*, 428, 3121  
Navarro, J. F., Frenk, C. S., & White, S. D. M. 1997, *ApJ*, 490, 493  
Okabe, N., Futamase, T., Kajisawa, M., & Kuroshima, R. 2014, *ApJ*, 784, 90  
Peng, C. Y., Ho, L. C., Impey, C. D., & Rix, H.-W. 2002, *AJ*, 124, 266  
Peng, E. W. & Lim, S. 2016, *ApJ*, 822, L31  
Reines, A. E., Greene, J. E., & Geha, M. 2013, *ApJ*, 775, 116  
Roman, J. & Trujillo, I. 2016, arXiv:1603.03494  
Smith, R., Sánchez-Janssen, R., Fellhauer, M., Puzia, T. H., Aguerri, J. A. L., & Fariás, J. P. 2013, *MNRAS*, 429, 1066  
Taylor, C., Boylan-Kolchin, M., Torrey, P., Vogelsberger, M., & Hernquist, L. 2015, arXiv:1510.06409  
Taylor, E. N., Hopkins, A. M., Baldry, I. K., Brown, M. J. I., Driver, S. P., Kelvin, L. S., Hill, D. T., Robotham, A. S. G., et al. 2011, *MNRAS*, 418, 1587  
van der Burg, R. F. J., Muzzin, A., & Hoekstra, H. 2016, *A&A*, 590, A20  
van Dokkum, P. G., Abraham, R., Merritt, A., Zhang, J., Geha, M., & Conroy, C. 2015a, *ApJ*, 798, L45  
van Dokkum, P. G., Romanowsky, A. J., Abraham, R., Brodie, J. P., Conroy, C., Geha, M., Merritt, A., Villaume, A., et al. 2015b, *ApJ*, 804, L26  
Wolf, J., Martínez, G. D., Bullock, J. S., Kaplinghat, M., Geha, M., Muñoz, R. R., Simon, J. D., & Avedo, F. F. 2010, *MNRAS*, 406, 1220  
Xue, X. X., Rix, H. W., Zhao, G., Re Fiorentin, P., Naab, T., Steinmetz, M., van den Bosch, F. C., Beers, T. C., et al. 2008, *ApJ*, 684, 1143  
Yozin, C. & Bekki, K. 2015, *MNRAS*, 452, 937  
Zaritsky, D., Gonzalez, A. H., & Zabludoff, A. I. 2006, *ApJ*, 638, 725